BRNO UNIVERSITY OF TECHNOLOGY
VYSOKÉ UČENÍ TECHNICKÉ V BRNĚ

FACULTY OF MECHANICAL ENGINEERING
FAKULTA STROJNÍHO INŽENÝRSTVÍ

INSTITUTE OF AUTOMOTIVE ENGINEERING
ÚSTAV AUTOMOBILNÍHO A DOPRAVNÍHO INŽENÝRSTVÍ

ADVANCED SOLUTION TO PISTON ASSEMBLY DYNAMICS

POKROČILÉ ŘEŠENÍ DYNAMIKY PÍSTOVÉ SKUPINY

Ph.D. THESIS
TEZE DIZERTAČNÍ PRÁCE

AUTHOR — Ing. Jozef Dlugoš
AUTOR PRÁCE

SUPERVISOR — doc. Ing. Pavel Novotný, Ph.D.
ŠKOLITEL

OPPONENTS
OPONENTI

DATE OF DEFENCE
DATUM OBHAJOBY

KEYWORDS

Piston, Lubrication, Friction Loss, Multibody Dynamics, Internal Combustion Engines

KLÍČOVÁ SLOVA

píst, mazání, třecí ztráty, Multibody Dynamics, spalovací motory

PLACE OF ARCHIVATION

Brno University of Technology
Library of Faculty of Mechanical Engineering
Technická 2896/2
616 69 Brno

MÍSTO ULOŽENÍ PRÁCE

Vysoké učení technické v Brně
Areálová knihovna fakulty strojního inženýrství
Technická 2896/2
616 69 Brno

ISBN 80-214-
ISSN 1213-4198

CONTENTS

INTRODUCTION

Many manufacturers are currently restricted by national and international regulations imposed on their products. In case of internal combustion engine (ICE), one of the criteria is the amount of exhaust gas emissions. The monitored components are carbon monoxide CO, carbon dioxide CO_2, hydrocarbons HC, nitrogen oxides NO_x and particulate matter. Emission standards have been commonly established in the European Union (EU) as well as in the other countries worldwide. The emissions of air quality pollutants have been continuously decreased thanks to increasingly stringent emission limits.

There are several ways of reducing the fuel consumption, hence emissions, such as reduction of overall weight of the vehicle and reduction of loss—improving the efficiency of combustion process, reducing aerodynamic drag, reducing friction forces in powertrain, etc. In terms of friction loss of ICE, the piston assembly is one of the main contributors [1].

On 1 July 2016, Regulation (EU) No 540/2014 entered into force. This Regulation permits the sound level of motor vehicles from 74 dB to 68 dB until 2026. Motivation for this regulation is improvement of public health. Traffic noise causes harm to health in numerous ways. Protracted noise-related stress can exhaust human physical reserves, disrupt the regulatory capacity of organ functions and hence limit their effectiveness. Traffic noise is a potential risk factor for development of medical conditions and incidents, such as high blood pressure and heart attacks [2]. Noise of ICE related to the piston is often lower than legislative standards. However, this noise is very user-unfriendly, and therefore its early identification and elimination is required.

1 PROBLEM DEFINITION AND DOCTORAL THESIS GOALS

The piston manufacturers face challenging tasks during development of the piston: to propose several piston designs and to select the best one which fulfils the following requirements:

- High structural strength
- Low friction
- Low wear
- Light weight
- Low oil consumption
- Low pollutant emission values
- Low price

These requirements are contradictory. Ideally, the design excellence is an optimal compromise which achieves the best parameters. This is a typical problem for optimization methods. If the optimal design is to be found in real time, the solution to objective function has to be fast enough. Experimental methods often do not meet this criterion, so computational methods are preferred. The complexity of the computational model affects the solution speed and accuracy. Unfortunately, this is a trade-off problem as well.

During development of the piston, it is important to find the relation between the change of the design and the behaviour of the piston (friction loss, vibrations, piston secondary motion, wear, etc.). The development process consists of comparison of a remarkable number of designs. Therefore, it is essential to have a tool which is able to quickly and accurately compare the individual designs and thus provide needed feedback.

The objective of this doctoral thesis is to develop an advanced computational tool for the solution to the dynamics and tribology of the piston assembly. The computational tool has to include proper computational models that are able to capture the physics which affect the piston the most, for example, real piston and liner shape, piston and liner temperature deflection, elastic deformation and different lubrication regimes. Since the computational tool is meant to be used by the piston manufactures, it has to be fast and accurate enough. In order to validate the computational tool, the simulated results have to be compared with the experimental results. The following text describes the solution to these demanding doctoral thesis goals.

2 SIMULATION MODEL

During the operating cycle, the piston is performing reciprocating motion in liner axis direction (primary motion), lateral motion (u_{lat}) in direction perpendicular to the piston pin axis and rotational motion (α_{tilt}) in plane perpendicular to the piston pin axis (secondary motion). In addition to these motions, the piston moves transversally (u_{tran}) in direction of the piston pin axis (tertiary motion). Sign convection of the piston secondary and tertiary motion is depicted in Figure 1.

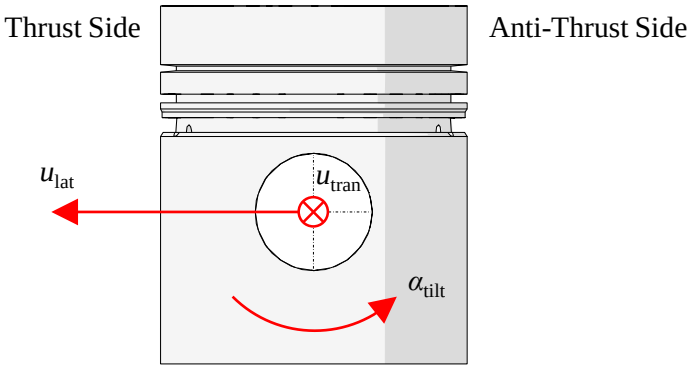

Figure 1 Piston Secondary and Tertiary Motion Sign Convection

The piston is exerted to the inertia forces, the gas pressure forces, the contact forces, the friction forces and the moments which result in the piston secondary and tertiary motion. Therefore, it is essential to accurately estimate these forces and moments in order to predict the piston motion correctly.

The strategy of the development of the computational model is based on the commercial Multibody Dynamics (MBD) software, namely Adams/View by MSC Software. This software solves general problems of dynamics (it is not limited to the automotive only). Its big benefit is that it can be easily augmented by algorithms—user-written subroutines—coded in C++ or Fortran. User-written subroutines are computational models representing physical laws, which are inevitable to simulate the piston to liner interaction correctly.

2.1 PISTON TO LINER GAP

The distance between the piston and the liner h is one of key parameters which affect the behaviour of this contact pair significantly. The distance consists of several components:

$$h = \sum_{i=1}^{7} h_i \tag{1}$$

Where h_1 is the rigid component, h_2 is the piston skirt shape, h_3 is the liner shape, h_4 is the thermal deformation of the piston, h_5 is the thermal deformation of the liner, h_6 is the piston deformation and h_7 is the liner deformation.

2.2 SOLUTION TO HYDRODYNAMICS

The piston to liner contact exists through the lubrication oil or by asperities. The ratio of these two contributors defines the lubrication regime:

- Hydrodynamic lubrication
- Partial (mixed) lubrication
- Boundary lubrication

2.2.1 HYDRODYNAMIC LUBRICATION REGIME

The hydrodynamic lubrication regime occurs when both contact surfaces are fully separated by the continuous fluid film and the oil flow is not affected by the surface roughness. This is true when the ratio between the nominal film thickness h and the composite surface roughness σ is significantly larger than 3 [3].

This regime may be described by the Reynolds equation of the following form:

$$\frac{\partial}{\partial x}\left(\frac{\rho h^3}{12\eta}\frac{\partial p}{\partial x}\right)+\frac{\partial}{\partial y}\left(\frac{\rho h^3}{12\eta}\frac{\partial p}{\partial y}\right)=\frac{U}{2}\frac{\partial(\rho h)}{\partial y}+\frac{\partial(\rho h)}{\partial t} \tag{2}$$

The left side terms of the Reynolds equation (2) are Poiseuille terms (describing the lubricant flow caused by the pressure gradient), the first right side term is Couette term or wedge term (describing the lubricant flow caused by the viscous drag force acting on the fluid caused by the relative movement of the surfaces) and the last right side term is squeeze term (describing the flow caused by the squeeze effects). Shear stress caused by the hydrodynamic lubrication is:

$$\tau=-\frac{\eta U}{h}\pm\frac{h}{2}\frac{\partial p}{\partial y} \tag{3}$$

2.2.2 PARTIAL LUBRICATION REGIME

If the nominal film thickness h is getting thinner and the following inequation is satisfied:

$$1<\frac{h}{\sigma}\leq 3 \tag{4}$$

the lubricant flow is affected by the surface roughness and the mixed lubrication regime occurs. Patir and Cheng [3] derived the so-called Average Reynolds equation:

$$\frac{\partial}{\partial x}\left(\phi_x\frac{\rho h^3}{12\eta}\frac{\partial \bar{p}}{\partial x}\right)+\frac{\partial}{\partial y}\left(\phi_y\frac{\rho h^3}{12\eta}\frac{\partial \bar{p}}{\partial y}\right)=\frac{U}{2}\frac{\partial(\rho \bar{h}_T)}{\partial y}+\frac{U}{2}\sigma\frac{\partial(\rho\phi_s)}{\partial y}+\frac{\partial(\rho \bar{h}_T)}{\partial t} \tag{5}$$

Equation (5) involves flow factors denoted by label ϕ with subscript representing the type of the flow factor. In general, the flow factors compare the flow in a rough bearing to that of a smooth bearing. They depend on the distance of the surfaces, the statistical properties of the combined roughness and in specific cases (shear flow factor and shear stress factor) even on the statistical parameters of each surface separately. Increasing the distance between the contact surfaces, the impact of the flow factors decreases and becomes negligible.

Similar to the mean oil flow, the mean hydrodynamic shear stress is augmented by the surface roughness influence:

$$\tau = -\frac{\eta U}{h}\left(\phi_{\mathrm{f}} \pm \phi_{\mathrm{fs}}\right) \pm \phi_{\mathrm{fp}} \frac{h}{2}\frac{\partial \overline{p}}{\partial y} \tag{6}$$

2.2.3 BOUNDARY LUBRICATION REGIME

The boundary lubrication regime may be distinguished by the dominant contact of the asperities of rough surfaces (this mechanism is in limited portion present in the partial lubrication regime as well). It occurs when the nominal surface film thickness is less than the combined surface roughness. The most widespread theory of the rough surface contact was conceived by Greenwood and Tripp [4] in 1970. They derived the equation for contact pressure determination of the following form:

$$p_{\mathrm{c}} = \frac{8\pi}{5}\eta_{\mathrm{r}}\beta\sigma K F_{5/2} \tag{7}$$

Equation (7) represents the dependence of the contact pressure p_{c} on the nominal surface distance h. Various contact model theories differ in the form of this dependence. The MBD computational model can be fed with any of such contact models as long as it behaves reasonably.

In boundary lubrication regime, the Coulomb's law of friction is valid:

$$F_{\mathrm{asp,f}} = f_{\mathrm{dry}} F_{\mathrm{asp,n}} \tag{8}$$

2.2.4 NUMERICAL SOLUTION

The computational model uses the Average Reynolds equation (5) which becomes the Universal Reynolds equation (2) for higher film thickness values. The Reynolds equation is a nonlinear partial differential equation (PDE). The proposed computational model employs the Finite Difference Method (FDM) for the discretization of the Reynolds equation. The solution is found by Gauss-Seidel iteration method augmented by Successive Overrelaxation (SOR) parameter.

The cavitation (local evaporation of the lubricant and subsequent implosion of bubbles caused by the drop in fluid pressure) is implemented in the Reynolds equation by the Reynolds exit boundary condition.

2.3 MAPPING

The contact computational grid (for the estimation of the contact forces between the piston and the liner) is located on the piston and moving with the piston. The piston is moving relative to the liner, so the piston and the liner computational grids change their overlap during the operation cycle. The contact forces are dependent on the state of the piston and the state of the liner near the piston. The contact forces act only on the liner surface near the piston. Therefore, it is inevitable to map the current liner state (deformation, temperature, etc.) near the piston onto the contact computational grid attached to the piston. Afterwards, the contact forces are calculated and then mapped onto the computational grid of the liner in order to calculate the deformation, the wear and the engine block reaction.

2.3.1 SHAPE, TEMPERATURE AND DEFORMATION MAPPING

The piston and the liner shape, temperature and deformation are defined in each node of the piston and the liner computational grids. Since the overlap of these grids changes during the solution, discrete function of these variables is to be replaced by the continuous function—a job for a cubic spline. In this case, the Cubic Hermite spline is employed (third-order polynomials). The spline passes through a set of control points f_{00}, f_{01}, f_{10} and f_{11}:

$$f(t,u) = \begin{bmatrix} g_{00} \\ g_{01} \\ g_{10} \\ g_{11} \end{bmatrix}^{\mathrm{T}} \begin{bmatrix} f_{00} & f_{01} & s_{00} & s_{01} \\ f_{10} & f_{11} & s_{10} & s_{11} \\ l_{00} & l_{01} & k_{00} & k_{01} \\ l_{10} & l_{11} & k_{10} & k_{11} \end{bmatrix} \begin{bmatrix} h_{00} \\ h_{01} \\ h_{10} \\ h_{11} \end{bmatrix} \tag{9}$$

Square matrix of equation (9) depends on the control points f_{ij} and its derivations k_{ij}, l_{ij} and s_{ij}. If there is no change of the values of the control points (no deformation considered), the rest of the matrix cells are calculated only once during the simulation. Otherwise, the square matrix has to be recalculated with each update of the values of the control points.

2.3.2 FORCE MAPPING

The contact forces calculated for each node of the contact computational grid have to be mapped on the computational grid of the liner. This kind of mapping has different requirements than the mapping of the shape, temperature and deformation presented in the previous section. The overall source force effects should equal the overall target force effects. In other words, the static

equivalence between the source and the target object is crucial. The analytical integration of the pressure distribution fulfils this demanding requirement.

The bilinear shape functions are used for the creation of the analytical function, based on the discrete solution to contact computational grid:

$$f(t,u) = f_{00}N_{00} + f_{01}N_{01} + f_{10}N_{10} + f_{11}N_{11} \qquad (10)$$

Shape functions N_{ij} have a suitable form for the following analytical integration. The shape function N_{ij} takes the value of 1 for node [i, j], while it takes the value of 0 for other nodes, see (Figure 2).

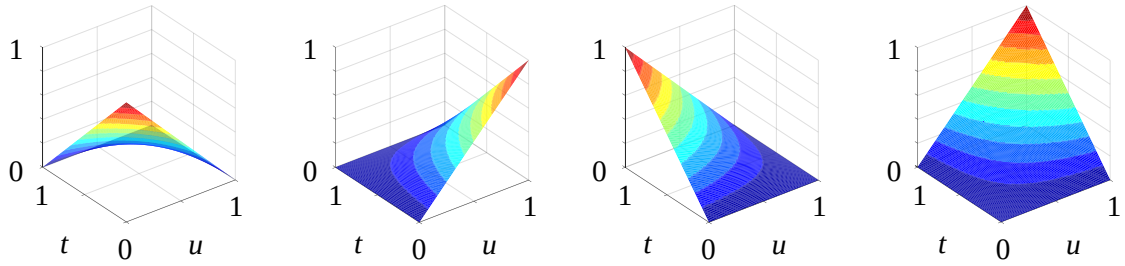

Figure 2 Bilinear Shape functions

Figure 3 shows envelopes of the piston skirt surface in red and the liner surface in black. The pressure distribution of the piston computational grid is defined by equation (10). In order to estimate the force in the node [I, J] of the liner computational grid, one has to integrate the pressure distribution of the piston computational grid in the region of the half grid near the node [I, J].

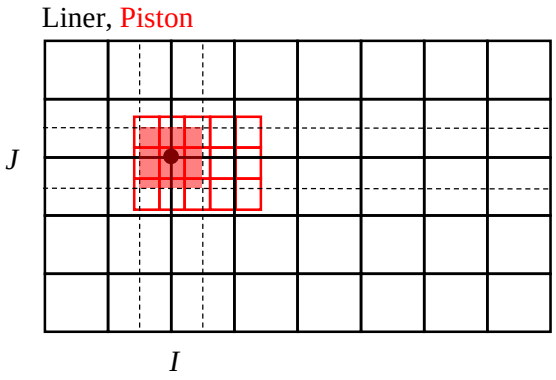

Figure 3 Mapping by Analytical Integration

Since the function *f(t,u)* is bilinear, numerical integration is trivial. In addition, the static equivalence between the source and the target object is preserved.

The mapping by the analytical integration was primary intended for the communication between the computational grid of the piston and the computational grid of the liner. However, such

mapping can be used for information exchange between the contact computational grid (hydrodynamic and asperity contact forces) and the piston computational grid (deformation). This is very beneficial, since the grid size requirements for the contact forces and for the deformation differ heavily. The partially-flooded piston skirt requires fine grid to solve the hydrodynamics and asperity contact forces accurately. On the contrary, the coarse structural mesh of the piston skirt is sufficient enough to capture the piston skirt deformation.

3 EXPERIMENTAL VALIDATION

Developed computational model could not be created without a certain level of simplification. Therefore, the question about the validity of the computational algorithms arises. The answer is offered by comparison with the experimental measurement. One has to be cautious here. The measured data often contains other corrupting effects, and the information can be easily lost.

3.1 EXPERIMENTAL MEASUREMENT

The piston geometrical position in the plane can be uniquely determined by the measurement of three different piston points using laser displacement sensors (Figure 4). The piston secondary motion is then derived from processing of the sensors' signal.

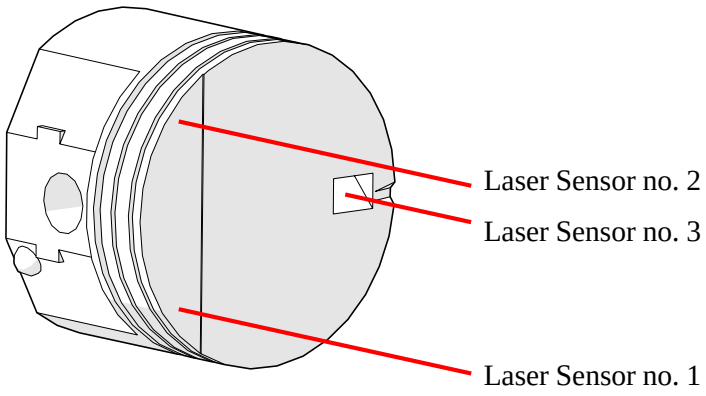

Figure 4 Measured Points on Piston Crown

The piston position is measured relatively to the laser displacement sensors location, which are not attached to the engine. Therefore, there is no need to separate the piston or liner shape. On the other hand, if the engine moves relatively to the laser displacement sensors' location (engine vibrations), this effect is reflected in the output signal as the piston secondary motion. In addition, the piston crown has to be detectable by the laser displacement sensors. Therefore, the convention cylinder head has to be removed. This disadvantage can be overcome by the use of sidevalve (SV) engine with transparent cylinder head. This method appears to provide the best price-performance ratio and therefore it is chosen for the validation of the developed computational model.

The measurement of the piston secondary motion by laser displacement sensors is applied on the ICE with SV type of valvetrain—Briggs & Stratton Series 500 type 10T5020139H1YY7001 (Table 1). It has simple cylinder head design with two main functions: to seal the combustion chamber and to carry the spark plug. It does not contain any valves, valve guides, rocker arms or camshaft as in case of OHC and OHV valvetrains. The transparent cylinder head allows the measurement of the piston axially loaded by the pressure in the combustion chamber (Figure 5). Therefore, Original Equipment Manufacturer (OEM) cylinder head is replaced with the transparent head made of the cast Plexiglas, while the combustion chamber shape is preserved.

Table 1 Test Engine Parameters

Engine Type	Briggs & Stratton Series 500
Rated Power	N/A
Torque	6 Nm
Displacement	158 cm^3
No. of Cylinders	1
Valvetrain	SV
Bore	65.1 mm
Stroke	47.7 mm

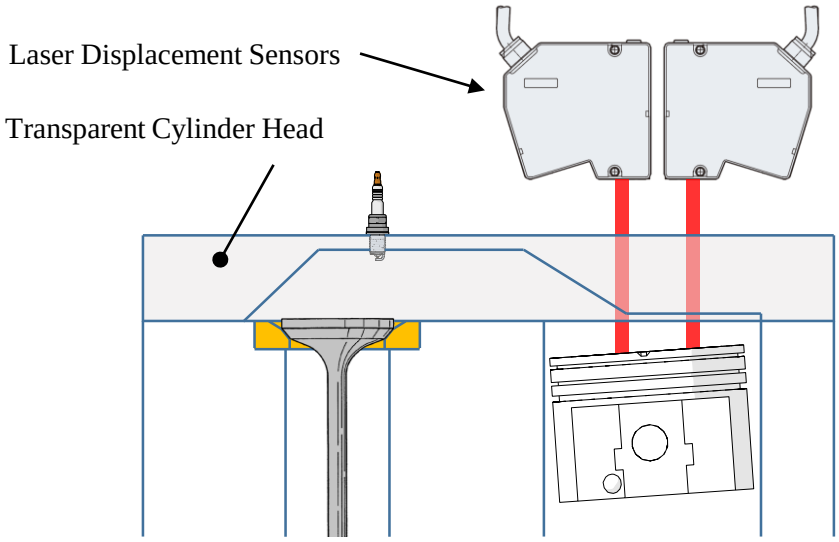

Figure 5 Measurement of Piston Secondary Motion thru Transparent Cylinder Head

Figure 6 and Figure 7 depict the test rig assembly and sensor mounts. The electric motor drives the SV engine via the V-belt. Three laser displacement sensors are attached to aluminum plate which is connected via the rotational head to the translational mount. This arrangement allows the calibration of the sensors' position in all 6 DOF.

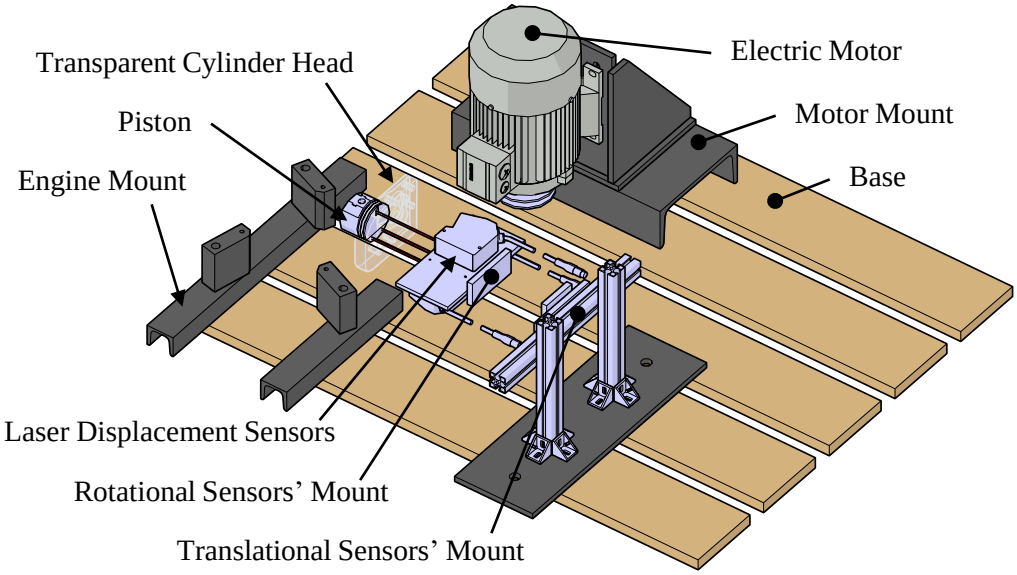

Figure 6 Test Rig Assembly

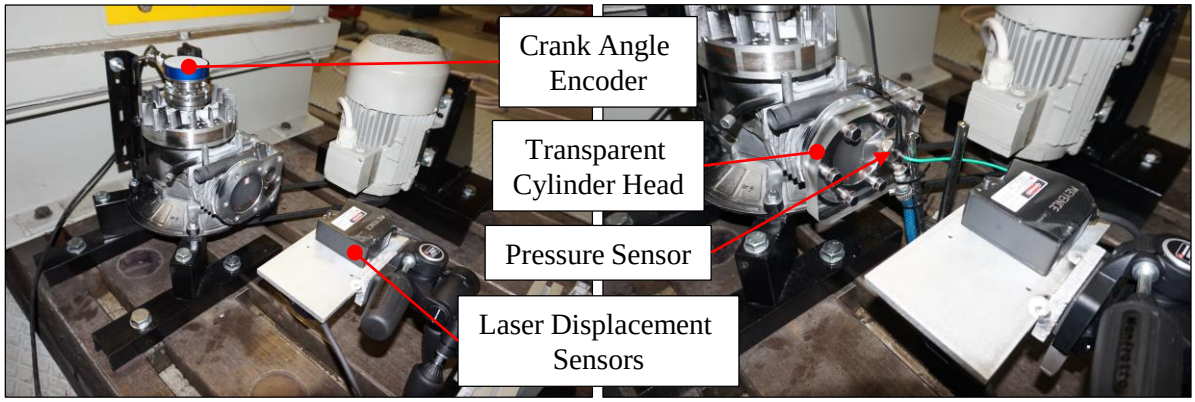

Figure 7 Sensor Mounts

3.2 DATA HANDLING

One measurement contains series of 100 operation cycles. For further data processing, the average of all these cycles is calculated. If an operation cycle is corrupted (incorrect trigger identification), it is excluded from the average calculus.

The end of the compression stroke is defined at 360° crank angle. Figure 8 shows the variation of the measured piston secondary motion. Thick curves stand for the average values while the interval bounded by thin curves represents the area of 68% probability of the occurrence of the measured data (with the assumption of normal distribution). The graphs show that the sample standard deviation in the Bottom Dead Centre (BDC) at the end of the expansion stroke is significantly higher than at the rest of the cycle. This is caused by occasional sensor failures at these intervals.

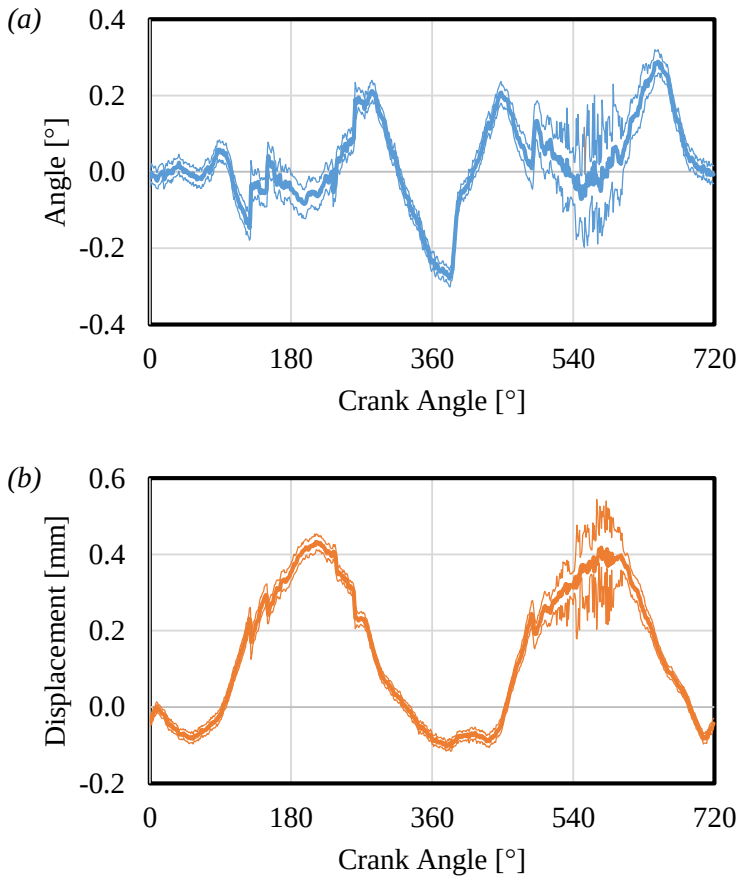

Figure 8 Variations of Measured (a) Piston Tilt Angle and (b) Piston Lateral Motion

The piston lateral motion depicted in Figure 8 (b) has amplitude of 0.267 mm. The nominal radial clearance between the piston and liner is 0.053 mm. In other words, indirectly measured piston lateral motion is affected by some parasitic effect.

Several analyses and measurements were performed in order to find the principal reason of measuring the amplitudes of the piston lateral motion which exceed the nominal radial clearance. The impact of deformation, the presence of transparent object between the sensors and the target and the engine vibrations were investigated. But still, none of these effects were arrested for doing the crime. One way or another, measured piston lateral motion is excluded from further analyses which are performed only on measured piston tilt angle.

3.3 RESULTS

The following data are measured and computed for the rotational speed of 1,108 rpm (Figure 9). The operation cycle may be divided to numerous regions. During intake down stroke (0° to 180° crank angle), the computed piston tilt angle shows a similar trend to the measured one, but values differ significantly. When the piston is in BDC, the distance between the piston and the laser displacement sensors is the largest. This affects the accuracy of the measurement in this portion of the cycle—occasional sensor failures at these intervals occurred. The differences

between computed and measured piston tilt angles decrease during the intake stroke. After reaching the Top Dead Centre (TDC), the piston changes its inclination from anti-thrust side toward thrust side for both cases. This very good agreement between computed and measured results lasts till the end of expansion stroke. During exhaust stroke, the differences increase again. At the beginning of this stroke, the computational model predicts the piston to be tilted toward thrust side and then it changes its tilt angle toward anti-thrust side. But the measurement shows that the piston is tilted toward thrust side steadily. Generally speaking, the most significant differences between the computational model and the measurement occur when the side force is small.

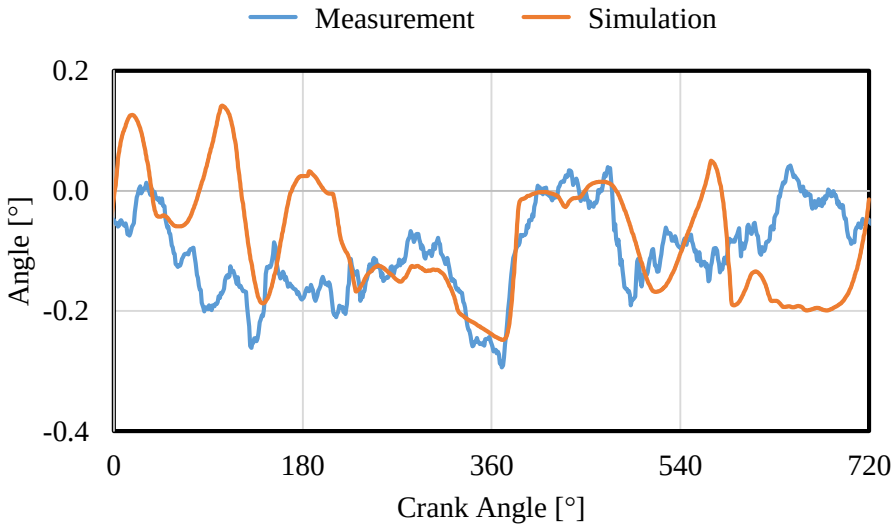

Figure 9 Measured and Computed Piston Tilt Angle for 1,108 rpm

3.4 CONCLUSIONS

Several other cases were measured and the following was observed. The greatest differences between the experiment and the computational model occur during compression stroke and exhaust stroke, when the side force is small. On the other hand, very good agreement is present during upper compression stroke and expansion stroke, especially for lower rotational speeds of the crankshaft. Higher speed causes reduced measurement accuracy or failure of the laser sensors when piston is in BDC.

Despite the above mentioned discrepancies and differences, it can be concluded that the developed computational model represents investigated effects adequately and the applied boundary conditions lead to reasonable results.

Levers to palliate the differences between the experiment and the computational model are the following. First of all, more accurate input parameters are required, for example, oil viscosity, oil temperature, oil film thickness and pressure acting on the piston. Their values may be measured or calculated reversely by optimization tools.

The measurement of oil viscosity is a standardized process. However, oil viscosity has to be used concurrently with oil temperature, which is different for the piston and liner surface and for the oil pan. Therefore, the measurement of the liner temperature should be conducted.

The measurement of the oil film thickness is very demanding. For such purposes, experimental engines using 2D laser induced fluorescence (LIF) are employed. More advanced solution to hydrodynamics (respecting mass conservation law) able to calculate current oil film thickness could do the job as well.

The gas pressure is measured in the combustion chamber. However, the pressure in the crankcase is also loading the piston. When the engine is motored by the electric motor, the pressure in the combustion pressure does not reach high values and the crankcase pressure may have an influence on the piston secondary motion. In case of fired engine, the crankcase pressure is negligible.

4 PARAMETER STUDY

The simulation is performed with the following conditions: the rotational speed of the crankshaft is 2,000 rpm, imep is 598.00 kPa, there is no tertiary motion, the piston and the liner are rigid, oil viscosity grade is SAE 0W-30, oil temperature is 105 °C, coefficient of dry friction is 0.1, liner shape is ideal cylindrical and piston skirt is partially-flooded.

4.1 IMPACT OF OIL FILM THICKNESS

As discussed above, the amount of oil available on the piston skirt is variable and the piston skirt is not fully-flooded by the oil during the entire operation cycle. The inlet oil film thickness affects the piston secondary motion, hence friction loss, tremendously. Figure 10 and Figure 11 depict the piston secondary motion for fully-flooded and partially-flooded piston skirt (according to the oil film thickness in [5]). In both cases, the piston lateral motion reflects the direction of the side force. However, the partially-flooded piston is not damped by the thick oil film, so the motion of the piston is more rapid. This leads to higher impact velocities causing leveraged acoustic effects of the engine block. In addition, the bouncing of the piston occurs in lower up stroke. These effects can be clearly distinguished by the piston tilt angle in Figure 11.

In friction loss case, the lower oil film thickness increases fmep from 2.712 kPa to 4.533 kPa. In addition, the asperity contact occurs at around 580° crank angle—friction loss peak in Figure 12.

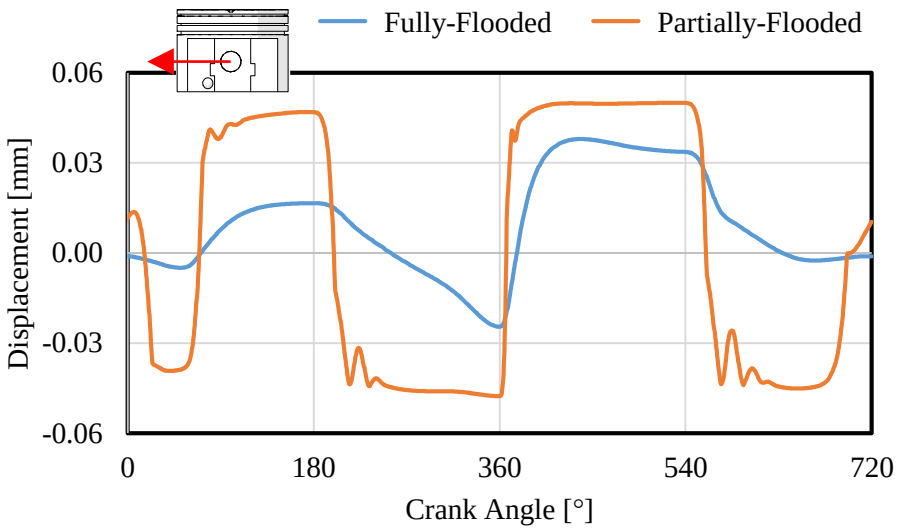

Figure 10 Piston Lateral Motion for Fully-Flooded and Partially-Flooded Piston Skirt

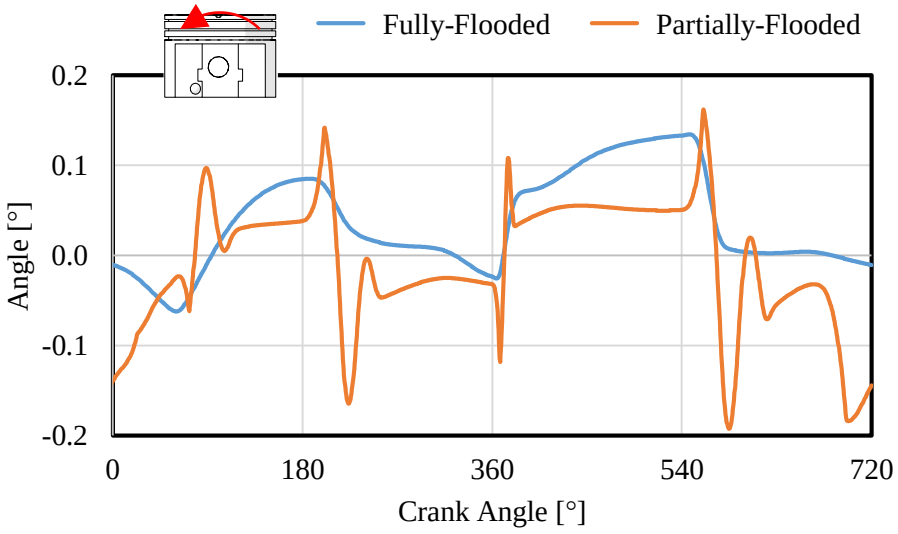

Figure 11 Piston Tilt Angle for Fully-Flooded and Partially-Flooded Piston Skirt

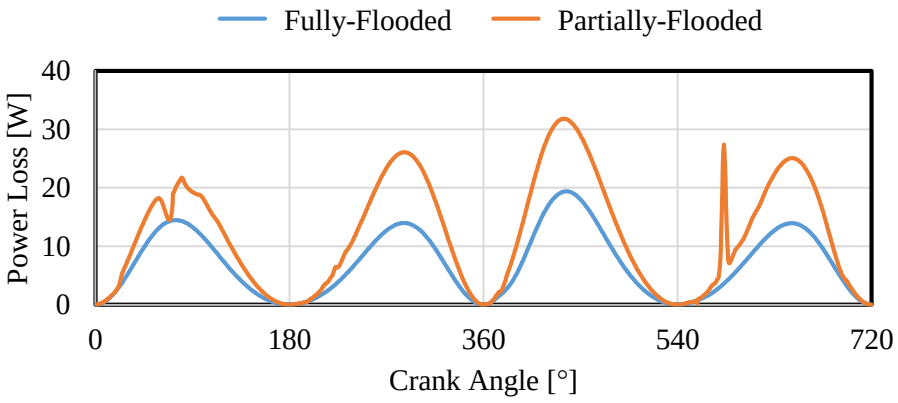

Figure 12 Overall Friction Loss for Fully-Flooded and Partially-Flooded Piston Skirt

4.2 Impact of Minimum Clearance Point

The measured piston shape has a minimum clearance point located below the level of the piston pin axis (Figure 13), where the side force acts. This causes positive piston tilting when the side force acts on the thrust side and negative piston tilting when the side force acts on the anti-thrust side. The picture is different when the minimal clearance point is located above the piston pin axis—the side force acting on the thrust side causes negative piston tilt angle and vice versa. To confirm this phenomenon, the measured piston shape (original) is mirrored according to the plane in the piston pin axis level—mirrored piston shape (Figure 13).

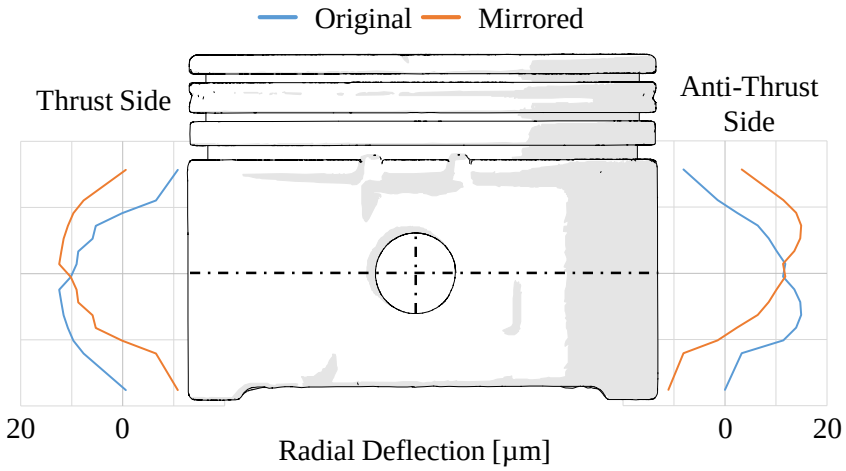

Figure 13 Original and Mirrored Piston Shape

Relocation of the minimum clearance point leads to the opposite trend of the piston tilt angle, as shown in Figure 14 and Figure 15. During compression stroke (180° to 360° crank angle), the side force is pushing the piston toward anti-thrust side. In case of the original piston shape, the minimum clearance point is below the piston pin axis level and therefore the piston is tilted toward anti thrust side. After reaching TDC (360° crank angle), the side force is pushing the piston toward thrust side and the tilt moment changes its direction as well. Therefore, the piston tilt angle is rapidly changed toward thrust side.

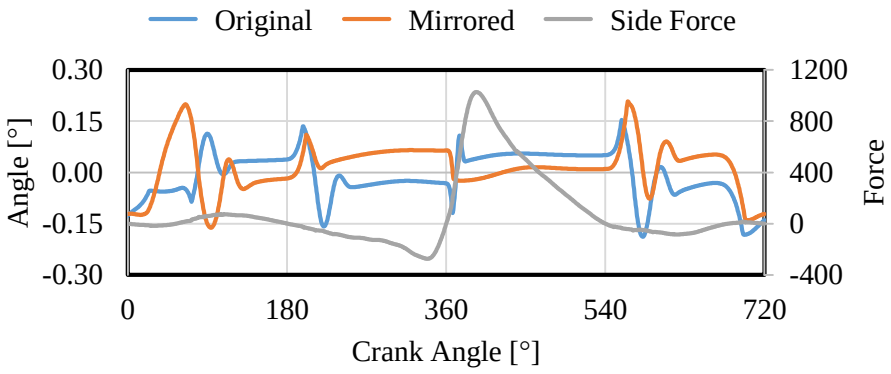

Figure 14 Piston Tilt Angle for Original and Mirrored Piston Shape and Corresponding Side Force

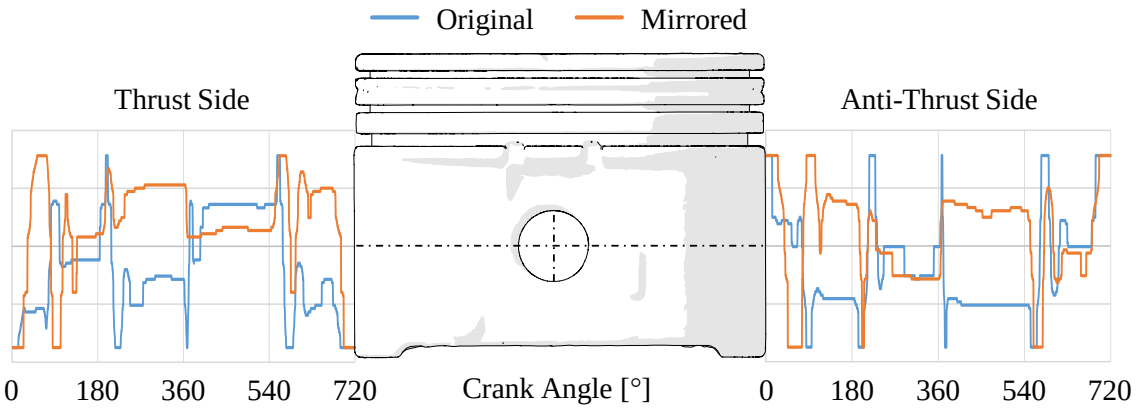

Figure 15 Location of Minimum Clearance Point for Original and Mirrored Piston Shape

4.3 IMPACT OF DEFORMATION

The piston skirt is loaded by the contact forces proportional to the side force. Therefore, the greatest deformation of the piston skirt occurs during the expansion stroke. This is illustrated on the results of the piston secondary motion in Figure 16 and Figure 17. After the ignition at around 360° crank angle, the thrust side of the piston skirt deforms significantly and allows an additional piston lateral motion. The deformation causes a formation of the flat region on the piston shape, and smaller piston tilt angle is present.

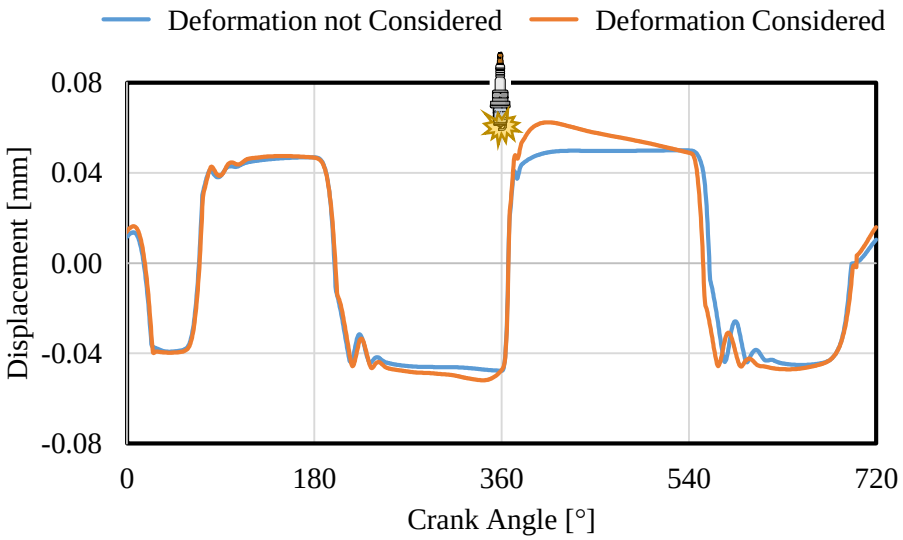

Figure 16 Piston Lateral Motion without and with Piston Deformation Considered

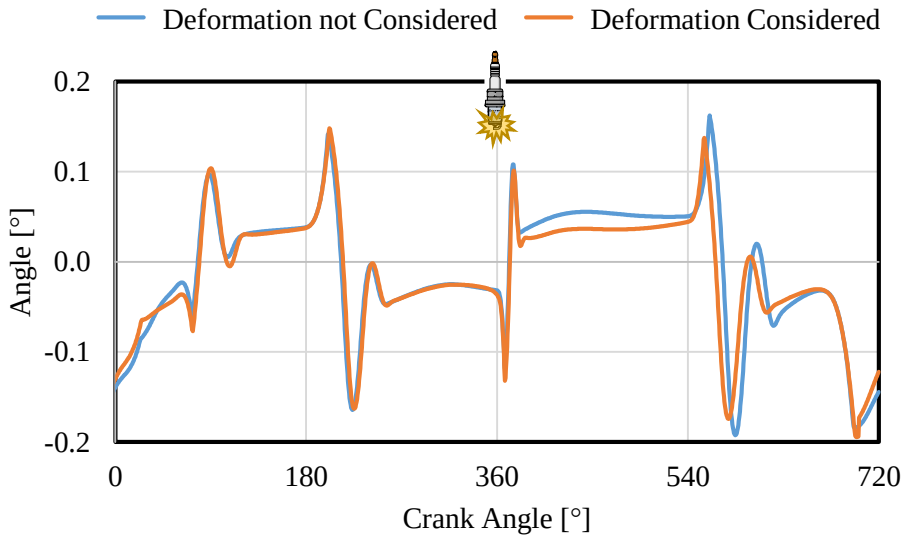

Figure 17 Piston Tilt Angle without and with Piston Deformation Considered

If the deformation of the piston is not considered, the minimal $\frac{h}{\sigma}$ ratio on thrust side has value of 3.15 at 439° crank angle (Figure 18). Allowing the deformation of the piston, this value is increased to 4.76 at 542.5° crank angle. There are two moments of the occurrence of the asperity contact on anti-thrust side (Figure 19) and they are caused by the edge contact of the piston skirt. The simulation with no piston deformation results in the minimal $\frac{h}{\sigma}$ ratios of 1.65 (222.5° crank angle) and 0.26 (583° crank angle) on anti-thrust side. Simulation with piston deformation considered leads to minimal ratios of 1.44 (226.5° crank angle) and 0.91 (583° crank angle).

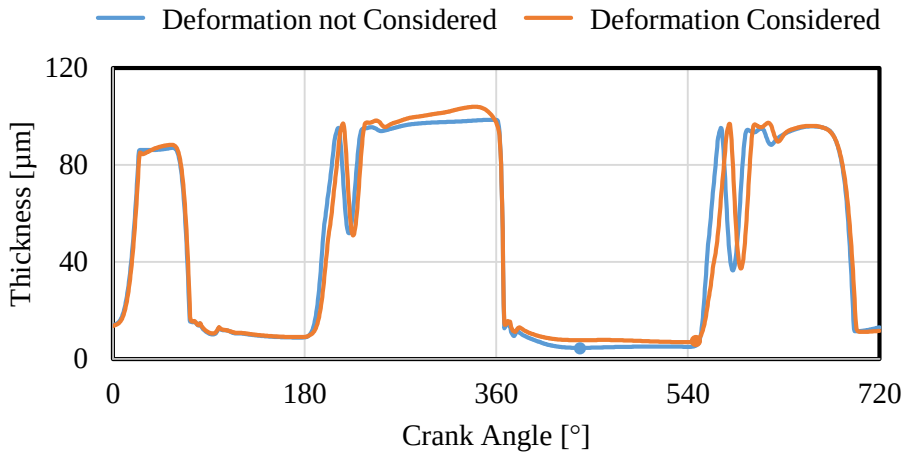

Figure 18 Minimum Oil Film Thickness on Thrust Side without and with Piston Deformation Considered

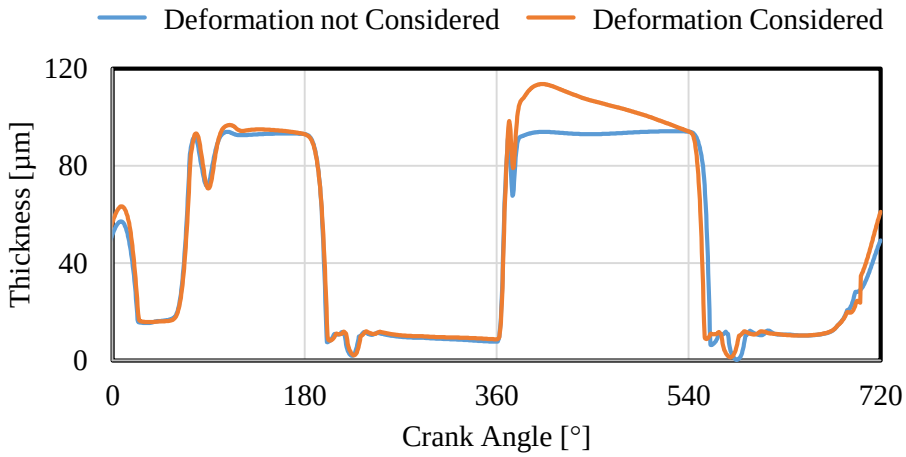

Figure 19 Minimum Oil Film Thickness on Anti-Thrust Side without and with Piston Deformation Considered

The deformed piston shape causes thicker oil film in expansion stroke so the friction loss (Figure 20) is decreased from fmep of 4.533 kPa to 4.498 kPa.

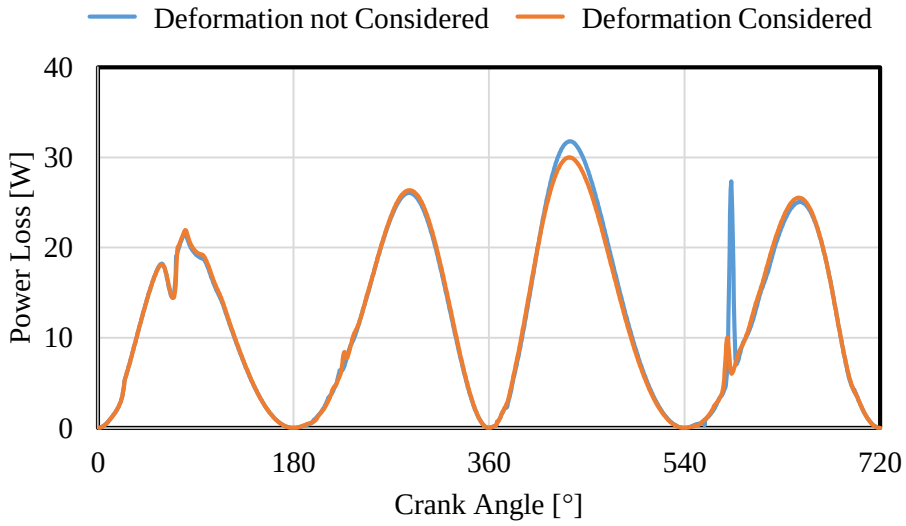

Figure 20 Overall Friction Loss without and with Piston Elastic Deformation Considered

5 SUMMARY

Each component of the ICE requires detailed study of its behaviour in order to find an optimal design and thus maximize the engine performance and minimize undesirable outputs. Piston is not an exception since it has heavy impact on friction loss, oil consumption, pollutant emissions, NVH effects, charge burn characteristics, etc. Therefore, deep analysis of the piston dynamics is inevitable. For this task, computational methods are more preferable; in most cases, they are faster and cheaper.

The first main goal of doctoral thesis was development of such computational tool for solution to the dynamics and tribology of the piston assembly. Here, it may be concluded that this goal is fulfiled by all means. The developed computational model is capable of considering:

- Hydrodynamic effects.
- Contact of asperities.
- Piston and liner shape.
- Piston and liner thermal deformation.
- Piston and liner deformation caused by contact forces and combustion process.
- Partially-flooded piston skirt.

In addition to these aspects, the computational model is able to work with different lubrication and structural grid sizes and is able of parallel computing. These enhancements lead to stable and effective solutions. Therefore, developed computational model can be used as a powerful engineering tool for optimization of the piston design.

The other main goal of this thesis was validation of the computational model by experiment. For this purpose, the measurement of the piston secondary motion (of SV engine with transparent cylinder head) by the laser displacement sensors is performed. The single-cylinder engine is driven by the electric motor and no combustion process is present. The measured piston lateral motion is corrupted for all measured cases. Numerous possible causes (deformation, distortion of the laser beam going through transparent object, engine vibrations, decreased accuracy of the sensors) of this phenomenon are investigated, but none of them are found guilty. However, the measured piston tilt angle reaches reasonable values and they agree well with the computed results when big side force is present—compression and expansion stroke.

Further improvements of computational tool still exist, for example, the introduction of GUI based creation of the model, the use of more advanced solution to hydrodynamics respecting mass conservation law, the calculation of shear-heating effects of the oil film, the more advanced calculation of wear and the NVH effects. In addition to these, the application of developed computational model on the pistons of modern engines would be beneficial.

REFERENCES

[1] HOPPE, St., R. MITTLER, T.H. DÖRNENBURG, and R. MESKE. Contribution of advanced piston and ring design and coatings on friction reduction in future diesel engines, 22nd Aachen Colloquium Automobile and Engine Technology, 2013.

[2] Regulation (EU) No 282/2014 of the European Parliament and of the Council of 11 March 2014 on the establishment of a third Programme for the Union's action in the field of health (2014-2020). Official Journal of the European Union. 2014.

[3] PATIR, Nadir and H. S. CHENG. An Average Flow Model for Determining Effects of Three-Dimensional Roughness on Partial Hydrodynamic Lubrication. Journal of Lubrication Technology. 1978, **100**(1), 12-17. DOI: 10.1115/1.3453103. ISSN 00222305.

[4] GREENWOOD, J. A. and J. H. TRIPP. The contact of two nominally flat rough surfaces. Proceedings of the Institution of Mechanical Engineers. London, 1970, **185**, 625-633. ISSN 0954-4100.

[5] BAI, Dongfang. Modeling Piston Skirt Lubrication in Internal Combustion Engines. Massachusetts, 2012. Dissertation. Massachusetts Institute of Technology.

CURRICULUM VITAE

– PERSONAL INFORMATION –

Born:	2nd May, 1991 in Trstená, Slovak Republic
Citizenship:	Slovak Republic
Nationality:	Slovak
Permanent Address:	Školská 311, 028 01 Brezovica, Slovak Republic
Email:	jozef.dlugos@hotmail.sk

– EDUCATION –

2014 – present	Brno University of Technology, Faculty of Mechanical Engineering, Institute of Automotive Engineering, doctoral study program
2012 – 2014	Brno University of Technology, Faculty of Mechanical Engineering, Institute of Automotive Engineering, master‘s study program
2009 – 2012	Brno University of Technology, Faculty of Mechanical Engineering, Institute of Automotive Engineering, bachelor’s study program

– WORK EXPERIENCE –

1/2018 – present	Brno University of Technology, Brno, Czech Republic Junior Researcher
2/2013 – 12/2014	Honeywell, HTS CZ, Brno, Czech Republic FEA Student Engineer

– PROJECT EXPERIENCE –

1/2018 – present	Development of Tools for Noise Vibration and Harshness Reduction of Turbochargers, Project ID: TJ01000033
9/2017 – present	Research of computational and experimental methods of mobile systems, Project ID: FSI-S-17-4104
1/2017 – 12/2017	Measurement of Piston Assembly Dynamics of Internal Combustion Engine, Project ID: FV 17-34
1/2016 – 12/2016	Analysis of Piston Assembly Dynamics of Internal Combustion Engines, Project ID: FV 16-39

ABSTRACT

The ultimate goal of this work is to develop an advanced computational model of piston assembly dynamics. The piston and the liner are interacting through the lubricant film or the surface asperities. This leads to different lubrication regimes and consequently different forces acting on the surfaces of the contact pair. During the solution to hydrodynamics and asperity contact forces, deformation of the piston and the liner has to be taken into account—the process is necessarily iterative in nature. Since the requirements for computational grid of the contact forces and of deformation differ, robust mapping algorithms are proposed.

The results of the developed computational tool are experimentally verified. For this purpose, the measurement of the piston secondary motion by laser displacement sensors is conducted. The measurement is done on the experimental sidevalve engine with transparent cylinder head in order to generate compression pressure in the combustion chamber. Measured piston lateral motion is corrupted. Therefore, only measurement of the piston tilt angle is further used. The agreement of the measured and computed results varies during the operation cycle. Good agreement is achieved for compression and expansion strokes. Oppositely, significant differences occur when the side force is small: intake and exhaust strokes.

Major contribution of this work is development of computational tool which implements the above mentioned effects that have a major impact on the piston assembly dynamics. Unfortunately, this leads to long computational times, especially when deformation is considered. For this reason, the parallel solution is developed. It is based on the parallelization of the subroutine during the evaluation of the sensibility analysis. This way, the solution time is reduced in order of magnitude.